



HAL
open science

Slow Dynamics of the Spin-Crossover Process in an Apparent High-Spin Mononuclear Fe(II) Complex

Yi Shan Ye, Xiu Qin Chen, You De Cai, Bin Fei, Pierre Dechambenoit, Mathieu Rouzieres, Corine Mathonière, Rodolphe Clérac, Xin Bao

► **To cite this version:**

Yi Shan Ye, Xiu Qin Chen, You De Cai, Bin Fei, Pierre Dechambenoit, et al.. Slow Dynamics of the Spin-Crossover Process in an Apparent High-Spin Mononuclear Fe(II) Complex. *Angewandte Chemie International Edition*, 2019, 58 (52), pp.18888-18891. 10.1002/anie.201911538 . hal-02418828

HAL Id: hal-02418828

<https://hal.science/hal-02418828v1>

Submitted on 19 Dec 2019

HAL is a multi-disciplinary open access archive for the deposit and dissemination of scientific research documents, whether they are published or not. The documents may come from teaching and research institutions in France or abroad, or from public or private research centers.

L'archive ouverte pluridisciplinaire **HAL**, est destinée au dépôt et à la diffusion de documents scientifiques de niveau recherche, publiés ou non, émanant des établissements d'enseignement et de recherche français ou étrangers, des laboratoires publics ou privés.

Slow Dynamics of the Spin-Crossover Process in an Apparent High-Spin Mononuclear Fe(II) Complex

Yi Shan Ye, Xiu Qin Chen, You De Cai, Bin Fei, Pierre Dechambenoit,^{id} Mathieu Rouzières, Corine Mathonière,^{id} Rodolphe Clérac^{*id} and Xin Bao^{*id}

Abstract: A mononuclear Fe(II) complex, that shows a high-spin ($S = 2$) paramagnetic behavior at all temperatures (with standard temperature scan-rates, $\approx 1 \text{ Kmin}^{-1}$), has indeed a low-spin ($S = 0$) ground state below 100 K. This low-spin state is not easily accessible due to the extremely slow dynamics of the spin-crossover process. Indeed, a full relaxation of the metastable high-spin state to the low-spin ground state takes more than five hours below 80 K. Bidirectional photoswitching of the Fe(II) state is achieved reproducibly by two selective irradiations (at 530-590 and 830-850 nm). The slow dynamics of spin-crossover and the strong structural cooperativity result in an unprecedented 95-K wide hysteresis loop induced by both temperature and selected light stimuli.

Some d^4 - d^7 metal ions, which exhibit the well-known spin-crossover (SCO) phenomenon, can be switched between high-spin (HS) and low-spin (LS) states by an external stimulus such as temperature, pressure, light, or magnetic field.^[1-5] The associated major changes of magnetic, optical and structural properties make these materials very promising for applications as molecular switches, in data storage devices and displays.^[6,7] In solid state, SCO is triggered by the metal ion coordination environment but is also influenced by the elastic interactions (i.e. cooperativity) between the magnetic centers. In case of strong cooperativity, SCO is always coupled to a first-order phase transition and thus to a slow kinetic of the spin-transition phenomenon.^[8] Therefore, the associated thermal hysteresis is always sensitive to the temperature scan-rate. An illustration of this dynamic effect in SCO systems is the possibility, in some cases, to thermally quench the high-temperature HS state by fast cooling and thus to kinetically suppress the spin-transition.^[9-14] Hence, it is important to emphasize that the scan-rate influence should be systematically investigated in potential SCO

complexes. Following this idea, Fe(II) complexes exhibiting an unexpected HS state at all temperatures have been often overlooked and often characterized by routine measurements. In rare examples, HS-Fe(II) complexes show a remarkable light bistability at low temperature with a photo-accessible LS phase that can be in turn reversibly photoconverted into the HS state. For instance, Gütlich, Hauser et al. described a $[\text{Fe}(\text{mtz})_6]^{2+}$ complex (mtz: methyltetrazole) containing two different Fe(II) sites: an LS site ($S=0$) and an HS site ($S=2$) at low temperature. Below 20 K, they performed two selective irradiations: one at 514 nm for the LS-to-HS conversion of the LS site, and the second at 830 nm for the HS-to-LS conversion of the HS site.^[15,16] These studies have been also completed for the $[\text{Fe}(\text{etz})_6]^{2+}$ complex (etz: ethyltetrazole)^[17,18] which shows a remarkable light-induced bistability of the HS sites. More recently, comparable bistability has been reported in a two-dimensional (2D) coordination polymer, $\{[\text{Fe}_{\text{HS}}(\text{bbtr})_3](\text{BF}_4)_2\}_\infty$ (bbtr: 1,4-di(1,2,3-triazol-1-yl)-butane),^[19-21] as well as in 2D HS:LS Hofmann-like frameworks^[22,23] and an Fe(III) SCO system.^[24]

Herein, we report a unique mononuclear Fe(II) complex for which its LS ground state is hidden below 100 K due to an unprecedentedly observed slow dynamics of the HS-to-LS SCO process. In contrast to the reported Fe(II) systems (i) with a classical SCO and thus a fast access to the LS ground state, or (ii) with an HS ground state showing photobistability (*vide supra*), the low-spin state of the present complex is thermally accessible below 80 K after a few hours of relaxation from the HS state.

Reaction of $\text{Fe}(\text{ClO}_4)_2 \cdot 6\text{H}_2\text{O}$, ^{2MeL} and NaNCBH_3 in CH_3OH results in a fast precipitation of $[\text{Fe}(\text{NCBH}_3)_2]$ (**1**) (^{2MeL}: *N,N'*-dimethyl-*N,N'*-bis(2-pyridylmethyl)-1,2-ethanediamine; see [Supporting Information, SI](#)). Single crystals suitable for X-ray diffraction were obtained by recrystallization from hot CH_3CN . The crystal structure was determined at 123 K (crystallographic data and refinement parameters are listed in [Tables S1](#) and [S2](#)). Complex **1** crystallizes in the monoclinic $C2/c$ space group and its molecular structure ([Figure 1](#)) is comparable to those of reported analogues based on related tetradentate ligands.^[25-27] The asymmetric unit contains half of a complex centered on a 2-fold axis. The tetradentate ligand wraps an Fe(II) metal ion in a *cis-α* conformation, leaving two *cis* positions for NCBH_3^- coligands. The average value of the six Fe–N bond lengths at 123 K ($\sim 2.19 \text{ \AA}$) falls within the range expected for octahedral HS-Fe(II) centers. Complexes are organized into flat layers in the *ab* plane dominated by van der Waals contacts between $\text{NCBH}_3 \cdots \text{H}$ atoms from the pyridine ring. Adjacent *ab* layers pack in a staggered fashion with $\pi \cdots \pi$ and $\text{NCBH}_3 \cdots \text{H}(\text{pyridine, methyl})$ short contacts (crystal packings: [Figures S3](#) and [S4](#); supramolecular interactions: [Table S3](#)).

Y. S. Ye, X. Q. Chen, Y. D. Cai, B. Fei, Dr. X. Bao
School of Chemical Engineering
Nanjing University of Science and Technology
210094 Nanjing, P. R. China
E-mail: baox199@126.com
Dr. P. Dechambenoit, M. Rouzières, Dr. Rodolphe Clérac
Univ. Bordeaux, CNRS, Centre de Recherche Paul Pascal - CRPP,
UMR 5031
33600 Pessac, France
E-mail: clerac@crpp-bordeaux.cnrs.fr
Dr. C. Mathonière
Univ. Bordeaux, CNRS, Institut de Chimie de la Matière Condensée
de Bordeaux - ICMCB, UMR 5026
33600 Pessac, France

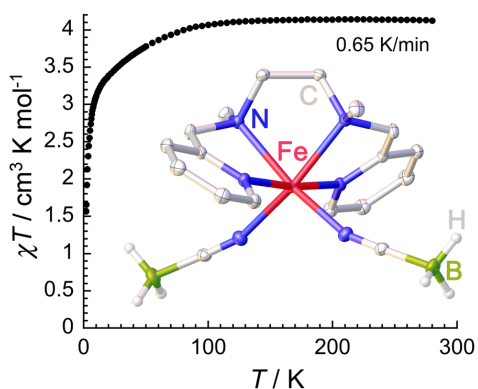


Figure 1. Temperature dependence of the χT product at 0.1 T for **1**. Inset: Molecular structure of **1** at 123 K with 50% probability thermal ellipsoids. ²M_eL hydrogens have been omitted for clarity.

Magnetic susceptibility (χ) measurements were recorded between 1.85 and 300 K on a polycrystalline sample of **1**. Its 300-K χT product is 4.12 cm³Kmol⁻¹ and remains relatively constant until 100 K (Figure 1), denoting the presence of an HS-Fe(II) complex (with $g \approx 2.3$). Below this temperature, χT decreases to 1.57 cm³Kmol⁻¹ at 1.85 K, due to the intrinsic magnetic anisotropy of the HS-Fe(II) sites and/or dipolar intermolecular antiferromagnetic interactions. Overall, the magnetic properties clearly show the presence of an HS-Fe(II) complex and the complete absence of a thermally driven SCO using standard temperature scan-rates (0.65 and 1.3 Kmin⁻¹).

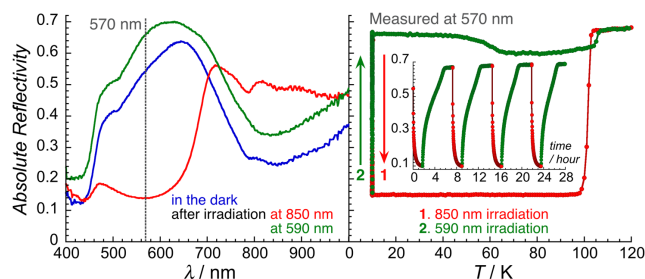


Figure 2. Left: Comparison of the reflectivity spectra at 10 K (reached from 270 K at 4 Kmin⁻¹ in the dark; blue) and after 100 minutes of successive 850-nm (red) and 590-nm (green) excitations (2 mWcm⁻²). Right: Thermal variation of the 570-nm reflectivity signal after irradiations at 850 nm (red; 2 mWcm⁻²) and after successive irradiations (2 mWcm⁻²) at 850 nm (red) and 590 nm (green) at 10 K. The inset shows the reversibility of the photoswitching at 10 K. A spectroscopic white light of 0.08 mWcm⁻² has been used.

Optical reflectivity spectra recorded between 270 and 10 K (Figure S5) are consistent with the magnetic data, showing a maximum around 850 nm in accord with the ⁵T₂→⁵E *d-d* transition of an HS-Fe(II) complex. Remarkably, **1** is very sensitive to light excitation in particular between 735 and 1050 nm as expected for an HS-to-LS photoconversion (Figure S6). As seen in Figures 2 and S7, an 850-nm irradiation at 10 K (1 hour) leads to a completely different spectrum (in red) with a 570-nm absorption typical of a LS-Fe(II) complex (tentatively assigned to both *d-d* and MLCT transitions). Upon subsequent

warming in dark (4 Kmin⁻¹), the reflectivity intensity at 570 nm increases sharply around 100 K, suggesting a LS-to-HS transition (right part of Figure 2, red dots). Furthermore, a 590-nm irradiation of the photogenerated LS phase leads to a completely recovery of the HS spectra (Figure 2). The LS and HS states can thus be reversibly and efficiently addressed by 590-nm and 850-nm irradiations over several cycles (Figure 2 inset and Figure S8). While the bulk magnetic measurements show that the HS state is observed over all temperatures (Figure 1), the surface reflectivity (at 570 nm) of the photogenerated HS state (right part of Figure 2, green dots) exhibits a small decrease around 55 K before recovering its HS value above 100 K. Such thermal evolution at the sample surface is reminiscent of the thermally-quenched or photo-induced metastable HS phases seen for SCO complexes, suggesting that below 100 K, the HS state is likely metastable while the LS phase is the ground state.

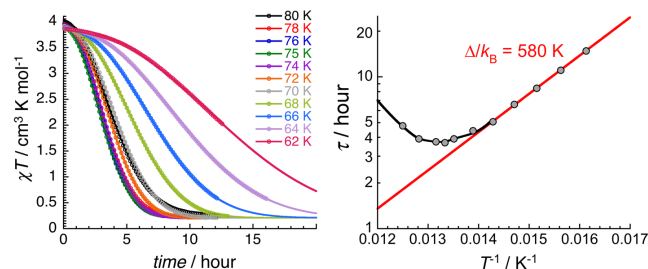


Figure 3. Left: Time evolution of the χT product at different temperatures reached in the dark at 5 Kmin⁻¹. The solid lines are the best fits discussed in the text. Right: τ versus $1/T$ plot. The red line is showing the Arrhenius behavior.

To test this hypothesis, the possible relaxation of the HS state at the bulk level was probed by magnetic measurements. Guided by the reflectivity study (right part of Figure 2, green dots), the isothermal decays of the χT product between 80 and 62 K were collected (Figure 3). As expected for a LS ground state, the χT product decreases systematically with time and reaches 0.21 cm³Kmol⁻¹ after several hours. The experimental data can be fitted well with stretched exponential functions (Table S4) leading to a relaxation time of the HS state, τ , which is close to 5 hours at 80 K. When lowering the temperature, τ decreases first to a minimum of 3.7(2) hours around 74-75 K and then increases exponentially below 70 K to reach 14.8 hours at 62 K (with an activation energy of 580 K; Right part of Figure 3). From this study, 74 K appears to be the optimized temperature for the fastest generation of the LS state at the bulk level. Optical reflectivity data at 74 K (Figure S9) confirmed this conclusion at the sample surface (3.2 hours), as the same spectrum is obtained after relaxation of the HS state or after photogeneration of the LS state (Figures S9, S10 and 2).

Following these relaxation experiments, the crystal structure of **1** was measured after 30 hours in the dark at 82 K (the lowest accessible temperature of our equipment). While the monoclinic C2/c space group is preserved (Table S1), the average Fe-N bond length decreases to 2.01 Å (Table S2), demonstrating the presence of LS Fe(II) centers. The reduction of the coordination sphere volume in the LS state results in the deformation of the tetradentate ligand (with larger displacements of the pyridines

than the aliphatic groups; Figures 4 and S11), as seen by the larger decrease of the distance between the pyridine N atoms (~ 0.34 Å) than between the amine N atoms (~ 0.12 Å). The SCO also induces a significant rearrangement of two NCBH_3^- ligands (Figure 4) with a displacement of the B atoms, which are ~ 0.61 Å closer in the LS state. As a consequence, the crystal lattice exhibits an anisotropic change of the unit cell during the HS-to-LS process (Table S1) with a and b parameters that reduce by ~ 0.63 and 0.05 Å, while, counter-intuitively, c expands by ~ 0.13 Å. Due to these large rearrangements of the structure, different atoms are involved in the van der Waals interactions of the two phases (Figure 4 and S11). The most remarkable illustration is the absence of short contact between NCBH_3^- and protons from the ethylene group in the HS phase while strong van der Waals interactions are present in LS state (about 0.2 Å shorter than the sum of van der Waals radii).

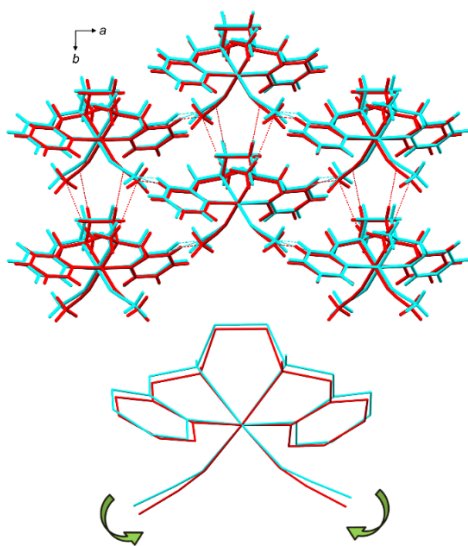


Figure 4. Overlay of crystal packing in the ab plane (top) and molecular structures (bottom) in **1** at 123 K (cyan) and 82 K (red). Van der Waals interactions are shown as thin dashed line.

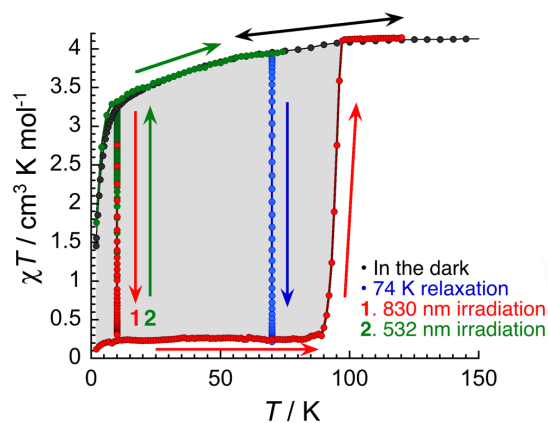


Figure 5. Temperature dependence of the χT product at 1 T for **1**: in the dark (black), during a 74-K relaxation (blue), during and after photoexcitations (heating at 0.4 Kmin^{-1} in the dark) at 830 nm (1. red; 2.5 mWcm^{-2}) and at 532 nm (2. green; 2 mWcm^{-2}) at 10 K.

Finally, the reversible photoswitching between LS and HS phases was also monitored by bulk photomagnetic measurements (Figure 5). Upon 830-nm light irradiation at 10 K, the χT product decreases with time and, after 45 minutes, reaches $0.3 \text{ cm}^3 \text{Kmol}^{-1}$ corresponding to an almost quantitative photoconversion (Figure S12). In the dark, this photoinduced LS information is erased above 95 K (increasing temperature at 0.4 Kmin^{-1}), leading to a giant light-induced hysteresis of about 95 K. The metastable HS state can be restored from the thermodynamic LS phase using a 532-nm irradiation as shown by the saturation of the χT product to $3.2 \text{ cm}^3 \text{K mol}^{-1}$ (Figures 5 and S12). Upon heating, the obtained χT data (in dark; at 0.4 Kmin^{-1}) are essentially identical to the one obtained upon cooling (at 0.65 Kmin^{-1}). At the bulk level, these photomagnetic measurements confirm unambiguously that the metastable HS state does not relax to the thermodynamic LS phase at this slow temperature scan-rate, which contrasts with the vast majority of the photo-active spin-crossover complexes. It is worth noting that the slight decrease around 60 K of the 570-nm optical reflectivity (right part of Figure 2) is thus only a surface effect.

Several factors certainly contribute in **1** to the extreme, and unusual, slow dynamics of the spin-crossover and its associated large activation energy (580 K, Figure 3). The important rearrangements of both crystal packing and Fe(II) coordination sphere, necessary for the SCO process to occur, are rendered difficult by a strong cooperativity, i.e. a dense network of supramolecular contacts between the switchable centers. The ligand field induced by the Fe(II) coordination sphere is also critical here as it leads to a spin-crossover process below 100 K, which does not allow the system to have enough thermal energy to overcome efficiently the energy barrier of 580 K. As expected the present results contrast with those of an isostructural pyrazine analogue, $[\text{Fe}^{(2\text{Me})\text{L}_{\text{pz}}}(\text{NCBH}_3)_2]$ ($^{2\text{Me}}\text{L}_{\text{pz}}$: N,N-dimethyl-N,N-bis(pyrazin-2-yl)methyl)-1,2-ethanediamine,²⁷ for which a stronger ligand field imposed by pyrazine groups induces a SCO at higher temperature (~ 168 K) without a particularly slow dynamics.

In conclusion, we reported a unique mononuclear Fe(II) complex with an extremely slow spin-transition and an unprecedented magnetic bistability with a 95-K wide hysteresis loop triggered by both temperature and selected irradiations. Even if the underlying mechanisms controlling these unusual dynamics are not clearly established yet, the stabilization of ligand fields associated with a low temperature SCO process (typically below 100 K) combined with strong supramolecular interactions should be the right ingredients to design new families of SCO complexes with reversible thermal- and photo-induced bistabilities over very large temperature domains.

Experimental Section

Experimental details on the syntheses are described in detail in the Supporting Information. TGA, PXRD pattern, crystal packing, additional reflectivity spectra of **1**, crystal data, refinement details and structural parameters can be found in the Supporting Informations.

Acknowledgements

This work was supported by the National Natural Science Foundation of China (21871140, 21401104) and the Priority Academic Program Development of Jiangsu Higher Education Institutions. C.M., R.C. and P.D. thank the University of Bordeaux, the CNRS, the Conseil Régional de Nouvelle Aquitaine, the MOLSPIN COST action CA15128 and the GdR MCM-2: Magnétisme et Commutation Moléculaires.

Conflict of interest

The authors declare no conflict of interest.

Keywords: Iron(II) • spin-crossover • slow dynamics
• thermally-induced bistability • photo-induced bistability

- [1] M. A. Halcrow, *Spin-Crossover Materials Properties and Applications*, John Wiley & Sons, Ltd., Chichester, **2013**.
- [2] P. Güttlich, H. A. Goodwin, in *Spin Crossover Transit. Met. Compd. I*, **2004**, pp. 1–47.
- [3] P. Güttlich, Y. Garcia, T. Woike, *Coord. Chem. Rev.* **2001**, *219*, 839–879.
- [4] J. A. Real, A. B. Gaspar, M. C. Muñoz, *Dalton Trans.* **2005**, 2062–2079.
- [5] A. Bousseksou, G. Molnár, L. Salmon, W. Nicolazzi, *Chem. Soc. Rev.* **2011**, *40*, 3313–3335.
- [6] J.-F. Létard, P. Guionneau, L. Goux-Capes, in *Spin Crossover Transition Metal Compounds III*, Springer-Verlag, Berlin/Heidelberg, **2004**, pp. 221–249.
- [7] O. Kahn, C. Jay Martinez, *Science* **1998**, *279*, 44–48.
- [8] S. Brooker, *Chem. Soc. Rev.* **2015**, *44*, 2880–2892.
- [9] M. Marchivie, P. Guionneau, J. F. Létard, D. Chasseau, J. A. K. Howard, *J. Phys. Chem. Solids* **2004**, *65*, 17–23.
- [10] V. Gómez, C. Sáenz de Pipaón, P. Maldonado-Illescas, J. C. Waerenborgh, E. Martin, J. Benet-Buchholz, J. R. Galán-Mascarós, *J. Am. Chem. Soc.* **2015**, *137*, 11924–11927.
- [11] N. Paradis, G. Chastanet, T. Palamarciuc, P. Rosa, F. Varret, K. Boukheddaden, J. F. Létard, *J. Phys. Chem. C* **2015**, *119*, 20039–20050.
- [12] N. Paradis, G. Chastanet, J. F. Létard, *Eur. J. Inorg. Chem.* **2012**, 3618–3624.
- [13] T. Delgado, A. Tissot, L. Guéneé, A. Hauser, F. J. Valverde-Muñoz, M. Seredyuk, J. A. Real, S. Pillet, E.-E. Bendeif, C. Besnard, *J. Am. Chem. Soc.* **2018**, *140*, 12870–12876.
- [14] J. Weihermüller, S. Schlamp, B. Dittrich, B. Weber, *Inorg. Chem.* **2019**, *58*, 1278–1289.
- [15] P. Poganiuch, S. Decurtins, P. Guetlich, *J. Am. Chem. Soc.* **1990**, *112*, 3270–3278.
- [16] R. Hinek, P. Gutlich, A. Hauser, *Inorg. Chem.* **1994**, *33*, 567–572.
- [17] A. Hauser, P. Güttlich, R. Hinek, H. Spiering, D. Schöllmeyer, *Chem. Eur. J.* **1996**, *2*, 1427–1434.
- [18] A. Hauser, R. Hinek, H. Spiering, P. Güttlich, *Chem. Eur. J.* **1996**, *2*, 1435–1439.
- [19] P. Chakraborty, R. Bronisz, C. Besnard, L. Guéneé, P. Pattison, A. Hauser, *J. Am. Chem. Soc.* **2012**, *134*, 4049–4052.
- [20] P. Chakraborty, S. Pillet, E. E. Bendeif, C. Enachescu, R. Bronisz, A. Hauser, *Chem. Eur. J.* **2013**, *19*, 11418–11428.
- [21] P. Chakraborty, C. Enachescu, A. Humair, L. Egger, T. Delgado, A. Tissot, L. Guéneé, C. Besnard, R. Bronisz, A. Hauser, *Dalton Trans.* **2014**, *43*, 17786–17796.
- [22] E. Milin, V. Patinec, S. Triki, E. E. Bendeif, S. Pillet, M. Marchivie, G. Chastanet, K. Boukheddaden, *Inorg. Chem.* **2016**, *55*, 11652–11661.
- [23] M. M. Ndiaye, S. Pillet, E.-E. Bendeif, M. Marchivie, G. Chastanet, K. Boukheddaden, S. Triki, *Eur. J. Inorg. Chem.* **2018**, *2018*, 305–313.
- [24] T. Boonprab, S. J. Lee, S. G. Telfer, K. S. Murray, W. Phonsri, G. Chastanet, E. Collet, E. Trzop, G. N. L. Jameson, P. Harding, D. J. Harding, *Angew. Chem. Int. Ed.* **2019**, *58*, 11811–11815.
- [25] J. Zhou, B.-W. Zhu, J. Luan, Z. Liu, J.-K. Fang, X. Bao, G. Peng, J. Tucek, S.-S. Bao, L.-M. Zheng, *Dalton Trans.* **2015**, *44*, 20551–20561.
- [26] J. Luan, J. Zhou, Z. Liu, B. Zhu, H. Wang, X. Bao, W. Liu, M.-L. Tong, G. Peng, H. Peng, et al., *Inorg. Chem.* **2015**, *54*, 5145–5147.
- [27] X. Liu, J. Zhou, X. Bao, Z. Yan, G. Peng, M. Rouzières, C. Mathonière, J.-L. Liu, R. Clérac, *Inorg. Chem.* **2017**, *56*, 12148–12157.

COMMUNICATION

An extremely slow spin-transition and an unprecedented magnetic bistability with a 95-K wide hysteresis loop triggered by both temperature and selected irradiations are observed in a unique mononuclear Fe(II) complex. This work describes the necessary ingredients to design new families of spin-crossover complexes with reversible thermal- and photo-induced bistabilities over very large temperature domains.



Yi Shan Ye, Xiu Qin Chen, You De Cai, Bin Fei, Pierre Dechambenoit, Mathieu Rouzières, Corine Mathonière, Rodolphe Clérac and Xin Bao**

Slow Dynamics of the Spin-Crossover Process in an Apparent High-Spin Mononuclear Fe(II) Complex

Supporting Information

Slow Dynamics of the Spin Crossover Process in an Apparent High-Spin Mononuclear Fe(II) Complex

Yi Shan Ye, Xiu Qin Chen, You De Cai, Bin Fei, Pierre Dechambenoit, Corine Mathonière,
Rodolphe Clérac* and Xin Bao*

General

All reagents obtained from commercial sources were used without further purification. Safety Note: Perchlorate salts are potentially explosive, and caution should be taken when dealing with such materials.

Synthesis of $[\text{Fe}^{(2\text{MeL})}(\text{NCBH}_3)_2]$ (**1**):

To a solution of $^{2\text{MeL}}$ ligand (0.027 g, 0.1 mmol) in CH_3OH (15 mL) was added $\text{Fe}(\text{ClO}_4)_2 \cdot 6\text{H}_2\text{O}$ (0.036 g, 0.1 mmol) and NaNCBH_3 (0.013g, 0.2 mmol). The resulting reaction mixture was stirred for 10 minutes and the yellowish precipitate was filtered. Recrystallization from hot CH_3CN gave yellowish block crystals in 51% yield. Selected IR spectroscopy (diamond ATR, cm^{-1}): 2349, 2318 (B-H), 2283, 2262, 2212, 2177 (vs, $\text{C}\equiv\text{N}$), 1606, 1483, 1440, 1303, 1118 (vs), 1080, 1060, 1022, 979, 817, 761(vs), 727; Elemental analysis, Calcd: C, 53.26; H, 6.95; N, 20.70. Found: C, 53.31; H, 6.69; N, 20.45.

Physical characterization

Magnetic susceptibility measurements of the reported Fe(II) complexes (14.09 mg of **1** sealed in a polypropylene bag ($3 \times 0.5 \times 0.2$ cm: 13.38 mg) were recorded with a Quantum Design MPMS-XL SQUID magnetometer, operating with applied fields up to 7 T at temperatures from 1.85 to 300 K. Prior to the experiments, the field dependent magnetization was measured at 100 K in order to detect the presence of any bulk ferromagnetic impurities. The samples appeared to be free of any significant ferromagnetic impurities. The photomagnetic experiments were performed using a set of photodiodes coupled via an optical fiber to the cavity of a MPMS-5S Quantum Design SQUID magnetometer. Samples of **1** were maintained in a straw between two thin layers of polyethylene films to limit orientation effects. Note that the temperatures have been corrected to consider the light irradiation heating (an average +2 K has been observed with red light). Experimental susceptibilities were corrected for sample holder and intrinsic diamagnetic contributions. TGA curve (Figure S1) was recorded on a Mettler-Toledo TGA / SDTA851e thermoanalyzer under a nitrogen atmosphere at a heating rate of 10 K min^{-1} . PXRD patterns shown in Figure S2 were recorded on a D8 ADVANCE X-Ray Diffractometer ($K\alpha$ radiation, $\lambda = 1.54056 \text{ \AA}$). Elemental analyses were performed using an Elementar Vario EL Elemental Analyser. IR spectra were recorded by the attenuated-total-reflectance (ATR) technique in the range $4000\text{--}650 \text{ cm}^{-1}$ using a Perkin-Elmer Spectrum. The surface reflectivity measurements have been performed with a home-built system, operating between 10 and 300 K and in a spectrometric range from $400\text{--}1000 \text{ nm}$. A halogen-tungsten light source (Leica CLS 150 XD tungsten halogen source adjustable from 0.05 mW cm^{-2} to 1 W cm^{-2}) was used as the spectroscopic light. The measurements were calibrated by baryum sulfate as reference sample. As the samples are potentially very photosensitive, the light exposure time was minimized during the experiments keeping the samples in the dark except during the spectra measurements when white light is shined on the sample surface ($P = 0.08 \text{ mW cm}^{-2}$). For all the excitation/de-excitation experiments performed at 10 K, the sample was initially placed at this temperature keeping the sample in the dark to avoid any excitation. Heating and cooling measurements were carried out at 4 K min^{-1} . For white light irradiation, the source described above was used, but in a continuous manner with a power of 0.08 mW cm^{-2} . Light Emitting Diodes (LEDs) operating between 365 and 1050 nm (from Thorlabs) were used for excitation experiments.

Single crystal X-ray diffraction

Single crystal X-ray data were collected with a Bruker APEX II Quasar diffractometer, equipped with a graphite monochromator centred on the path of MoK α radiation ($\lambda = 0.71073 \text{ \AA}$). A single crystal, made by recrystallization from hot CH₃CN, was coated with Cargille™ NHV immersion oil and mounted on a fiber loop, followed by data collection at 123 K. The crystal was then cooled down to 82 K and the relaxation from the HS to the LS state was monitored by checking the evolution of the unit cell with time. After 30 hours, a full data collection was performed. The program SAINT was used to integrate the data, which was thereafter corrected using SADABS [1]. The structure was solved using direct methods and refined by a full-matrix least-squares method on F^2 using SHELXL-2014 [2] and the graphical user interface WinGX [3]. Non-hydrogen atoms were refined anisotropically and hydrogen atoms were placed at calculated positions refined using idealized geometries (riding model) and assigned fixed isotropic displacement parameters. It is worth mentioning that the higher R_{int} and R_1 values at 82 K than at 123 K are due to some cracks of the crystal occurring upon cooling due to the first order phase transition. This alteration of the crystal was confirmed visually and by the reconstructed precession images. CCDC-1558295-1558296 contain the supplementary crystallographic data for this paper. These data can be obtained free of charge from The Cambridge Crystallographic Data Centre via www.ccdc.cam.ac.uk/data_request/cif.

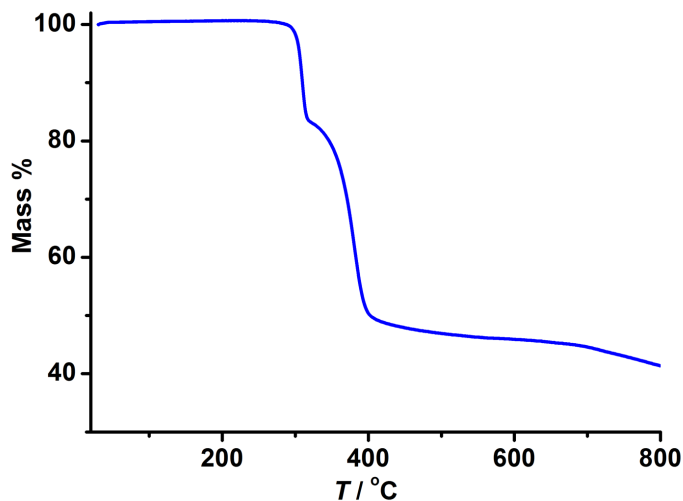


Figure S1. Thermogravimetric analysis (TGA) curves for **1** from 30 to 800°C at a 10 K min⁻¹ temperature rate under N₂ atmosphere. The result shows that complex **1** is stable up to 280°C (553 K). No weight loss was observed before decomposition, confirming the absence of interstitial solvent molecules.

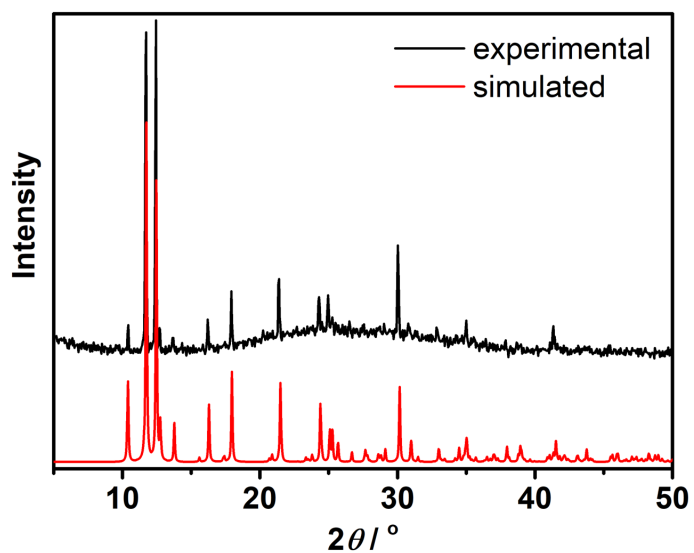


Figure S2. Comparison of the room temperature experimental PXRD pattern and the 123-K simulated one for **1**.

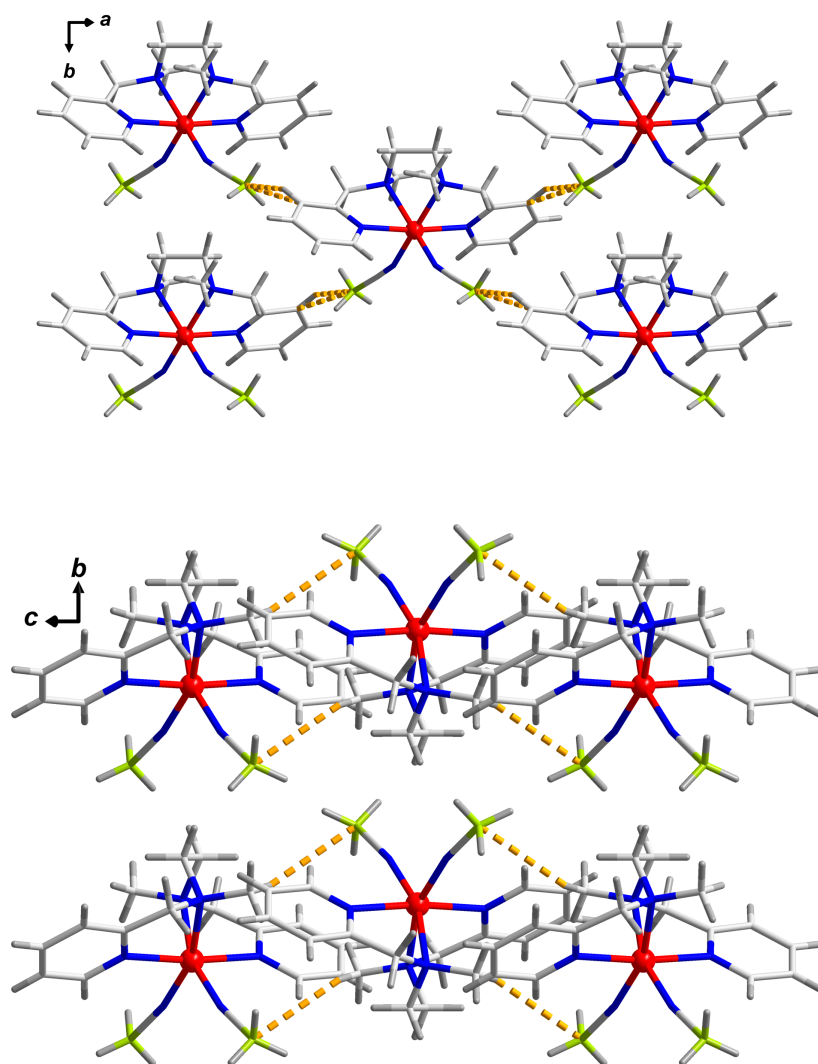


Figure S3. Packing diagrams of **1** at 123 K, showing the flat layer packed in the *ab* (top) and *bc* (bottom) planes. Color code: C, light grey; H, grey; Fe, red; N, blue; B, green. Short interactions are indicated by dotted yellow lines.

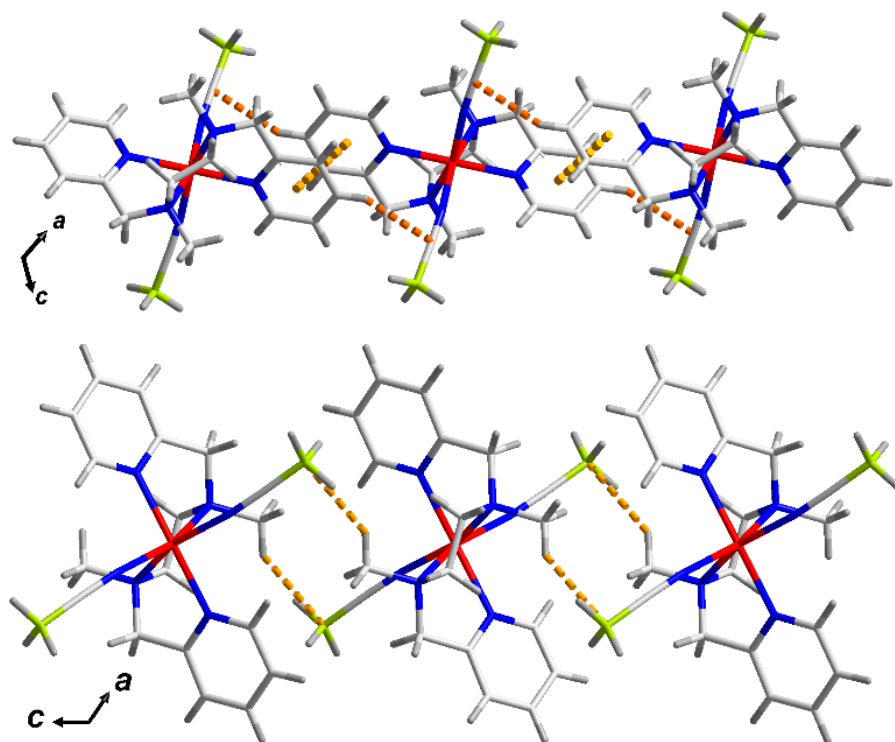


Figure S4. The 1D supramolecular arrangement of **1** at 123 K connected by $\pi\cdots\pi$ and $\text{NCBH}_3\cdots\text{H}(\text{pyridine})$ short contacts (top) and $\text{NCBH}_3\cdots\text{H}(\text{methyl})$ interactions (bottom). Color code: C, light grey; H, grey; Fe, red; N, blue; B, green. Short interactions are indicated by dotted yellow lines.

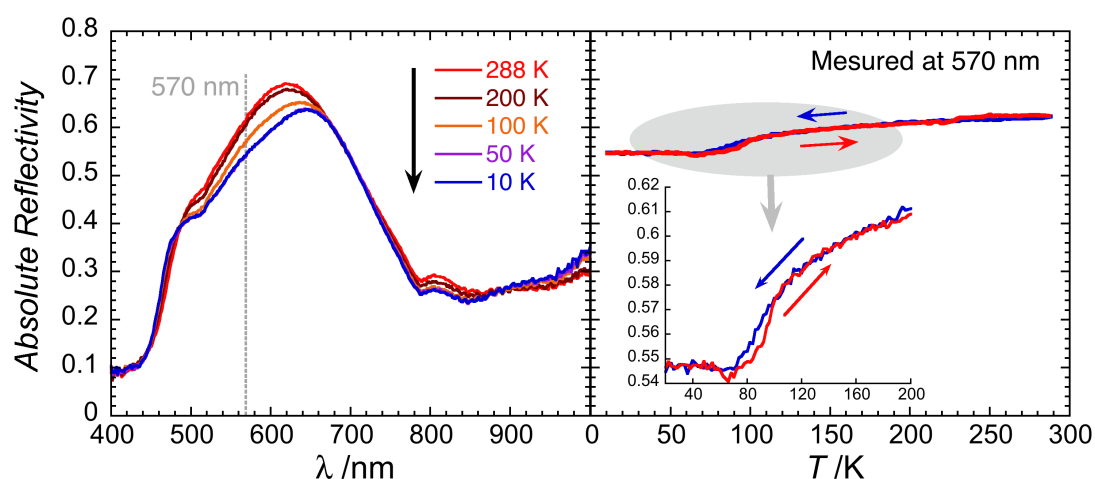


Figure S5. Left: Selected optical reflectivity spectra between 288 and 10 K recorded in the dark in cooling mode and at a scan rate of 4 K min^{-1} . Right: Thermal variation of the optical reflectivity signal recorded at 570 nm at a scan rate of 4 K min^{-1} . The small decrease of the intensity between 70 and 100 K might be related to a small amount of HS to LS conversion at the surface. A spectroscopic white light of 0.08 mW cm^{-2} has been used for these measurements.

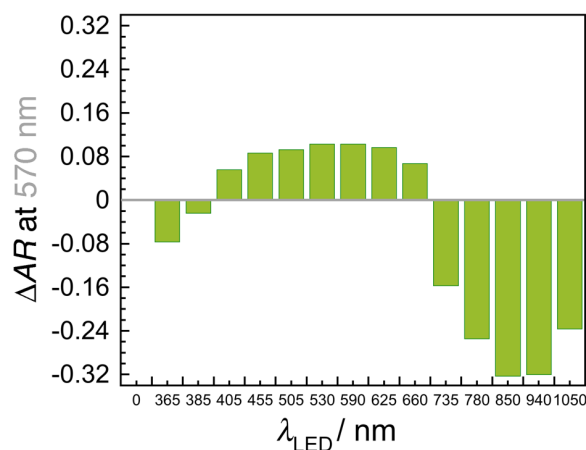


Figure S6. Variation of the absolute optical reflectivity (ΔAR) recorded at 570 nm and 10 K (after a fast cooling of the sample from room temperature) before and after excitation with different LEDs (10 minutes, at 2 mW cm^{-2}). A spectroscopic white light of 0.08 mW cm^{-2} has been used for these measurements.

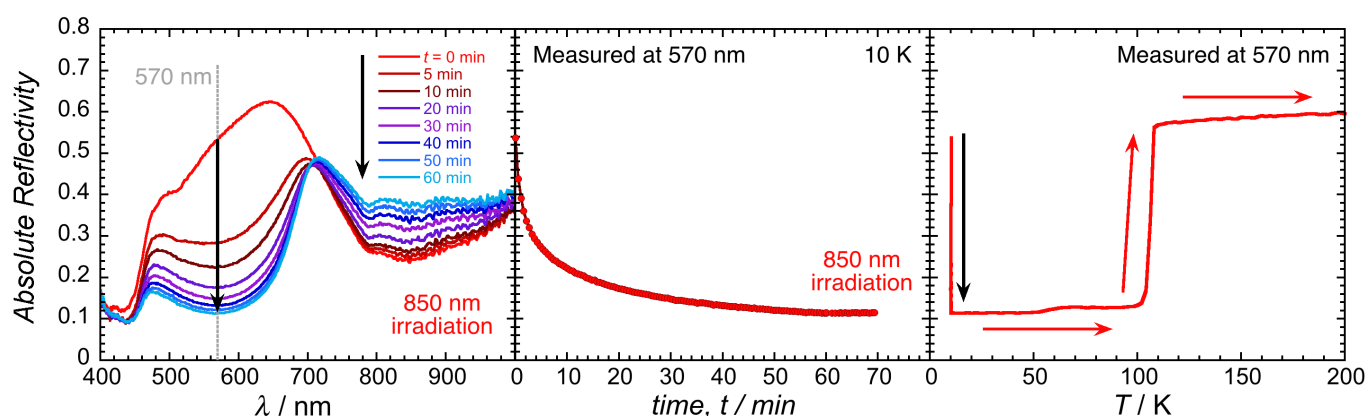


Figure S7. Left: Selected optical reflectivity spectra at 10 K (after a fast cooling of the sample from room temperature) as a function of the irradiation time with an 850-nm LED (at 2 mW cm^{-2}). Center: Time evolution of the optical reflectivity signal recorded at 570 nm and 10 K during an 850-nm LED irradiation (at 2 mW cm^{-2}). Right: Thermal variation of the optical reflectivity signal recorded at 570 nm in the dark after 70 minutes of an 850-nm LED irradiation at 10 K (the left and central figures show the photoinduced population of the LS state). A spectroscopic white light of 0.08 mW cm^{-2} has been used for these measurements.

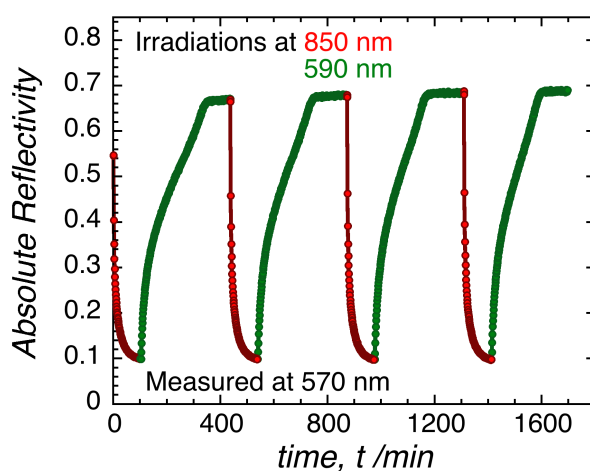


Figure S8. Time evolution of absolute optical reflectivity recorded at 570 nm under successive irradiations at 10 K (at 2 mW cm^{-2}) by 850-nm (in red) and 590-nm (in green) LEDs showing a very good reversibility of the photoinduced spin state switching. A spectroscopic white light of 0.08 mW cm^{-2} has been used for these measurements.

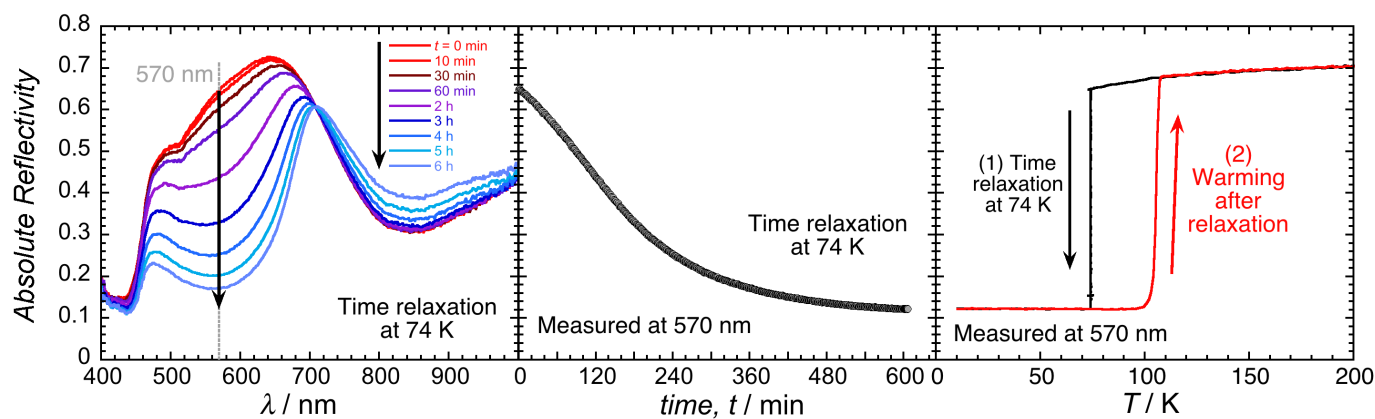


Figure S9. Left: Selected optical reflectivity spectra at 74 K (after a fast cooling of the sample from room temperature) as a function of time. Center: Time evolution of the optical reflectivity signal recorded at 570 nm and 74 K after a fast cooling of the sample from room temperature. Right: Thermal variation of the optical reflectivity signal recorded at 570 nm in the dark at 4 K min^{-1} : (1) in black, during the cooling of the sample from room temperature to 74 K and subsequent 10 hours of relaxation at 74 K (the left and central figures show the time population of the LS state) and (2) followed, in red, by the heating of the sample from 10 K to room temperature. A spectroscopic white light of 0.08 mW cm^{-2} has been used for these measurements.

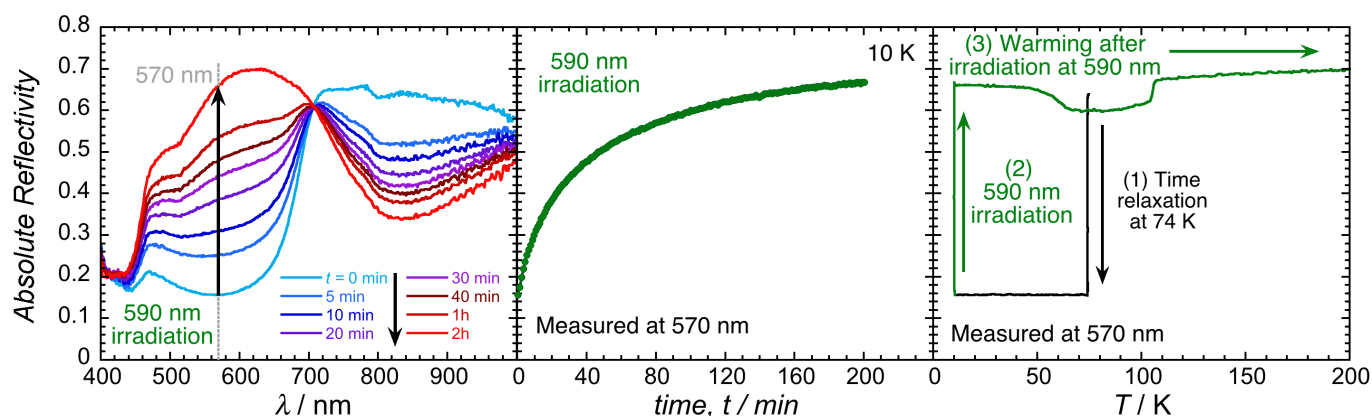


Figure S10. Before these experiments, the sample was prepared from room temperature, after a full relaxation to its LS state at 74 K and subsequent cooling to 10 K. Left: Selected optical reflectivity spectra at 10 K as a function of the irradiation time with a 590-nm LED (at 2 mW cm^{-2}). Center: Time evolution of the optical reflectivity signal recorded at 570 nm and 10 K during an irradiation at 590 nm (at 2 mW cm^{-2}). Right: Thermal variation of the optical reflectivity signal recorded at 570 nm in the dark at 4 K min^{-1} : (1) in black, during the cooling of the sample from room temperature to 74 K, subsequent 10 hours of relaxation at 74 K (Figure S9) and cooling to 10 K; (2) followed, in green, by an irradiation at 590 nm (at 2 mW cm^{-2}) of 4 hours and the heating of the sample from 10 K to room temperature. A spectroscopic white light of 0.08 mW cm^{-2} has been used for these measurements.

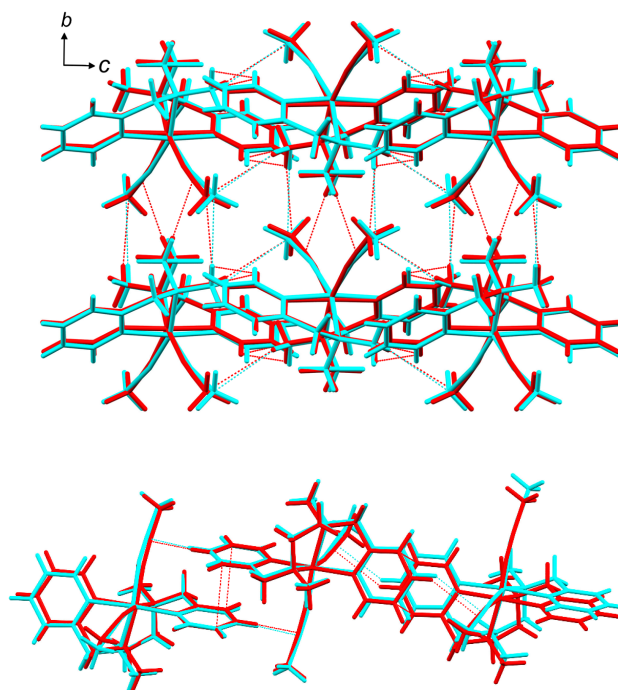


Figure S11. Overlay of (top) the crystal packing in the bc plane and (bottom) the π - π supramolecular chain (bottom) in complex **1** at 123 K (cyan) and 82 K (red). Van der Waals interactions are shown as thin dashed line.

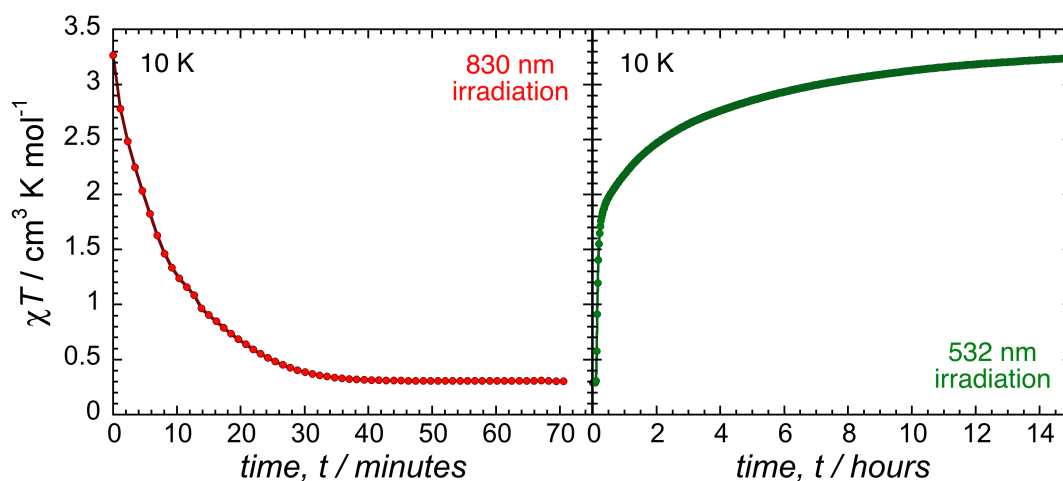


Figure S12. Time evolution of the magnetic susceptibility plotted as the χT product at 10 K under an 1-T magnetic field. Left, the χT product was measured after cooling down the sample to 10 K in the dark (at 1 K min^{-1}) and during an irradiation at 830 nm (at 2.5 mW cm^{-2}). As shown by the above plot, it takes about 45 minutes to fully photoinduce the thermodynamic LS state at the bulk level. Right, after cooling down the sample to 74 K from room temperature in the dark (at 1 K min^{-1}), a relaxation of 10 hours at 74 K and subsequent cooling down to 10 K in the dark (at 1 K min^{-1}), the χT product was measured during an irradiation at 532 nm (at 2 mW cm^{-2}). As shown by the above plot, it takes about 15 hours to almost fully photoinduce the metastable HS state at the bulk level.

Table S1. Crystal data and refinement details for **1**.

	[Fe(² MeL)(NCBH ₃) ₂] (1)	
Temperature / K	82	123
Empirical formula	C ₁₈ H ₂₈ FeN ₆ B ₂	C ₁₈ H ₂₈ FeN ₆ B ₂
Formula weight / g mol ⁻¹	405.96	405.96
Crystal system	Monoclinic	Monoclinic
Space group	C2/c	C2/c
<i>a</i> / Å	19.814(3)	20.4460(13)
<i>b</i> / Å	7.7387(10)	7.7897(5)
<i>c</i> / Å	15.570(2)	15.4415(11)
β / °	123.785(12)	123.940(5)
Volume / Å ³	1984.3(5)	2040.3(3)
<i>Z</i>	4	4
ρ_{calc} / mg mm ⁻³	1.359	1.321
μ / mm ⁻¹	0.775	0.754
<i>F</i> (000)	856.0	856.0
Reflections collected	24354	11558
Independent reflections	2809	2974
<i>R</i> _{int}	0.0854	0.0294
Goodness-of-fit on <i>F</i> ²	1.256	1.103
Final <i>R</i> indexes [<i>I</i> ≥ 2σ(<i>I</i>)]	<i>R</i> ₁ = 0.0808 <i>wR</i> ₂ = 0.1711	<i>R</i> ₁ = 0.0255 <i>wR</i> ₂ = 0.0695
Final <i>R</i> indexes [all data]	<i>R</i> ₁ = 0.0958 <i>wR</i> ₂ = 0.1768	<i>R</i> ₁ = 0.0277 <i>wR</i> ₂ = 0.0709
Largest diff. peak/hole / e Å ⁻³	1.52/−1.28	0.45/−0.19

Table S2. Selected bond lengths and structural parameters for **1**.

[Fe(^{2Me}L)(NCBH₃)₂] (1)		
<i>T</i> / K	82	123
Spin state	LS	HS
Fe-N _{NCBH₃} / Å	1.960(4)	2.1262(10)
Fe-N _{pyridine} / Å	2.016(3)	2.1875(10)
Fe-N _{amine} / Å	2.074(3)	2.2623(10)
Fe-N _{average} / Å	2.01	2.19
<i>cis</i> N-Fe-N / °	80.18(13)-98.29(13)	75.57(4)-104.66(6)
<i>trans</i> N-Fe-N / °	169.66(14)-177.9(2)	162.06(4)-173.74(5)
Σ Fe / °	57.7(11)	81.91(19)
Θ	174.5(17)	240.1(4)
N-C-B / °	174.6(4)	177.29(13)
Fe-N-C _{NCBH₃} / °	167.7(3)	162.55(10)

Table S3. Comparison of the intermolecular interactions in **1** at 82 and 123 K. Distances longer than the sum of van der Waals radii are underlined.

<i>T</i> / K	82	123
NCBH ₃ ⋯H(pyridine) / Å	2.9234(76)	2.8982(24)
NCBH ₃ ⋯H(methylene) / Å	2.6846(43)	<u>2.9023(14)</u>
NCBH ₃ ⋯H(methyl) / Å	3.031(5)	3.1447(17)
π⋯π (centroids) / Å	3.7094(4)	3.6254(11)
C(pyridine)⋯C(pyridine) / Å	3.3911(60)	<u>3.4229(21)</u>
C8(methyl)⋯H1(pyridine) / Å	2.8914(54)	<u>2.9509(17)</u>
H(methyl)⋯H(pyridine) / Å	2.3817(3)	<u>2.4084(1)</u>
H(methyl)⋯H(methyl) / Å	2.3933(4)	<u>2.6086(2)</u>
NCBH ₃ ⋯H(pyridine) / Å	2.8010(36)	2.8281(11)
NCBH ₃ ⋯H(methyl) / Å	3.1512(48)	3.0447(15)

Table S4. HS to LS relaxation time, τ , determined by fitting the experimental χT vs. time curves with a stretched exponential ($\chi T = \chi_0 T \exp(-(t/\tau)^\beta) + \chi_\infty T$ with $\chi_0 T = 3.70(6) \text{ cm}^3 \text{ K mol}^{-1}$, $\chi_\infty T = 0.210(5) \text{ cm}^3 \text{ K mol}^{-1}$, $\beta = 2.15(10)$; Figure 3 main text).

T / K	τ / hour	T / K	τ / hour
62	14.83	74	3.91
64	11.06	75	3.69
66	8.43	76	3.74
68	6.57	78	3.90
70	5.06	80	4.76
72	4.42		

References:

- [1] G. M. Sheldrick, SADABS Version 2.03, Bruker Analytical X-Ray Systems, Madison, WI, USA, 2000.
- [2] G. M. Sheldrick, *Acta Cryst.* **2015**, C71, 3-8.
- [3] L. J. Farrugia, *J. Appl. Cryst.* **2012**, 45, 849-854.